ARMY RESEARCH LABORATORY

Nondestructive Damage Characterization of Alumina Ceramics

by Raymond E. Brennan, James M. Sands, William H. Green, and Jian H. Yu

ARL-TR-4895 **July 2009**

NOTICES

Disclaimers

The findings in this report are not to be construed as an official Department of the Army position unless so designated by other authorized documents.

Citation of manufacturer's or trade names does not constitute an official endorsement or approval of the use thereof.

Destroy this report when it is no longer needed. Do not return it to the originator.

Army Research Laboratory
Aberdeen Proving Ground, MD 21005-5069

ARL-TR-4895 **July 2009**

Nondestructive Damage Characterization of Alumina Ceramics

Raymond E. Brennan
Oak Ridge Associated Universities

James M. Sands and William H. Green
Weapons and Materials Research Directorate, ARL

Jian H. Yu
Oak Ridge Institute for Science and Education

REPORT DOCUMENTATION PAGE	Form Approved OMB No. 0704-0188

1. REPORT DATE *(DD-MM-YYYY)*	2. REPORT TYPE	3. DATES COVERED (From - To)
July 2009	Final	January 2008–August 2008

4. TITLE AND SUBTITLE
Nondestructive Damage Characterization of Alumina Ceramics

5a. CONTRACT NUMBER

5b. GRANT NUMBER

5c. PROGRAM ELEMENT NUMBER

6. AUTHOR(S)
Raymond E. Brennan,* James M. Sands, William H. Green, and Jian H. Yu*

5d. PROJECT NUMBER
622618AH80

5e. TASK NUMBER

5f. WORK UNIT NUMBER

7. PERFORMING ORGANIZATION NAME(S) AND ADDRESS(ES)
U.S. Army Research Laboratory
ATTN: RDRL-WMM-D
Aberdeen Proving Ground, MD 21005-5069

8. PERFORMING ORGANIZATION REPORT NUMBER
ARL-TR-4895

9. SPONSORING/MONITORING AGENCY NAME(S) AND ADDRESS(ES)

10. SPONSOR/MONITOR'S ACRONYM(S)

11. SPONSOR/MONITOR'S REPORT NUMBER(S)

12. DISTRIBUTION/AVAILABILITY STATEMENT
Approved for public release; distribution is unlimited.

13. SUPPLEMENTARY NOTES
*Oak Ridge Associated Universities/Oak Ridge Institute for Science and Education, 4692 Millenium Drive, Ste. 101, Belcamp, MD 21017

14. ABSTRACT
A qualitative evaluation of surface and bulk damage and a quantitative percent damage assessment were used to compare the integrity of several nondestructive characterization techniques. X-ray digital radiography and ultrasound C-scan imaging were compared for their ability to detect damage in aluminum-backed alumina test samples. Incremental damage was produced by two different methods, including high-mass, low-velocity drop tower testing for large crack and low mass generation, and high-velocity fragment-simulating projectile testing for hairline crack generation. Surface damage was analyzed by visual inspection as a baseline before utilizing digital radiography and C-scan imaging. While both nondestructive techniques were able to detect the full extent of surface damage, C-scan imaging was more effective at detecting internal damage in the alumina samples, finding a significant number of cracks that were not detected through digital radiography. A corresponding assessment of a quantitative damage percent revealed higher and more accurate values from the C-scan images as compared to the digital radiography images due to the increased detection of bulk damage.

15. SUBJECT TERMS
impact testing, impact damage, ultrasound, digital radiography

16. SECURITY CLASSIFICATION OF:			17. LIMITATION OF ABSTRACT	18. NUMBER OF PAGES	19a. NAME OF RESPONSIBLE PERSON
a. REPORT	b. ABSTRACT	c. THIS PAGE			Raymond E. Brennan
Unclassified	Unclassified	Unclassified	UU	36	19b. TELEPHONE NUMBER (*Include area code*) 410-306-0878

Standard Form 298 (Rev. 8/98)
Prescribed by ANSI Std. Z39.18

Contents

List of Figures

List of Tables

INTENTIONALLY LEFT BLANK.

1. Introduction

It is a common practice in ballistic testing of armor materials to overmatch the test samples in order to determine the limits of their performance (*1–12*). The main goals of this work were to produce incremental levels of damage in armor ceramics using quasi-static methods and to characterize and compare the resulting damage using nondestructive means. Fracture of alumina structural armor ceramics was studied to determine the velocity and energy conditions under which different levels of damage were produced. The purpose of determining damage data, both qualitative and quantitative, was to gain a better understanding of the impact behavior of structural armor ceramics, which could also be used to provide input to impact and ballistic damage models.

Alumina test specimens were damaged by impact using two different quasi-static methods: drop tower testing and fragment-simulating projectile (FSP) testing. For drop tower testing, a high-mass indenter was used for low-impact velocity testing (*13*). By altering the drop tower height and the velocity and energy conditions, parameters that caused fracture were determined (*13*). For FSP testing, a low-mass projectile was utilized at high-impact velocities to determine the conditions that caused fracture. The two methods were chosen to compare relatively higher-mass, lower-velocity drop tower data to lower-mass, higher-velocity FSP data. The damage caused by these low- and high-velocity techniques was analyzed using nondestructive evaluation (NDE) methods.

Damage was determined by visually inspecting surface damage as well as using NDE methods including ultrasound (UT) testing and digital radiography (DR). A quantitative damage assessment comparing visual and nondestructive inspection was used to distinguish surface and bulk damage. The NDE methods were also compared to determine the effectiveness of bulk damage detection.

X-ray DR is a two-dimensional (2-D) projection radiology technique in the same category as film radiography and real-time radiography (*14–16*). Compared to other radiology techniques, DR has a significantly higher dynamic range and is able to produce digital images of the test specimens (*14–16*). These digital images can be enhanced, analyzed, compressed, archived, input as data to performance calculations, compared with digital data from other NDE modalities, or transmitted to other locations for remote viewing.

UT NDE uses the transmission of acoustic waves to nondestructively characterize a test specimen (*17–19*). Wave reflection is caused by acoustic impedance mismatch, which occurs at material boundaries (*17–19*). This can aid in detecting defects such as pores and inclusions. For C-scan imaging, an ultrasonic transducer is rastered over the desired sample area, and the collected signals from the A-scans, or amplitude scans, are assigned to x and y coordinates. The

changes in gated, or selected, reflected amplitude signals are evaluated. In this study, the bottom surface reflected signal was gated to study variations and look for distributed effects of inhomogeneities in the bulk of each sample. The reflected signal amplitude data, given in millivolts (mV), represented signal gain while the attenuation, given in decibels (dB), represented signal loss. These values were assigned to a color scale or gray scale that represented amplitude changes over the gated regions. The data were mapped according to the assigned scales and the x and y coordinates to produce bulk image maps of the samples. DR and UT C-scan imaging are complementary techniques that are capable of producing 2-D image maps of bulk features within a sample.

2. Experimental Test Specimens and Procedure

The samples used in this study were CoorsTek AD995 Al_2O_3 tiles (12.7 mm thick, 101.6 × 101.6 mm) adhesively bonded to aluminum backing plates (3.17 mm thick, 101.6 × 101.6 mm), Al 5083, which were used for structural support. They were made using a manual process in which a 2.5-mm-thick layer of GE Silicones SCS1000 sealant was applied to the backing layer and bonded to the ceramic tile. The bonding procedure utilized consistent application of the adhesive at a constant pressure (weight) to bond the backing plate to the ceramic during the 48-hr cure time. A total of 40 samples were fabricated.

Drop tower testing was conducted on samples 1–31 using an Instron Dynatup Model 8200 Impact Test Instrument. The instrument was utilized for high-mass drop weight impact testing with a 12.7-mm-diameter, high-strength steel hemispherical indenter (*13*). A 1077-g lead weight was added to the drop weight assembly, which included a 783-g, 10-kip, 7507 Charpy tup, a 1985-g frame, a 362-g front panel, a 362-g back panel, and various nuts and bolts, for a total drop weight of 3735 g. The initial drop heights covered a wide range, from 127 mm up to 1016 mm, where 1016 mm was the maximum height of the test instrument. The impact energies ranged from 4.57 J at a drop height of 127 mm to 37.19 J at a drop height of 1016 mm. Subsequent drop tests focused on a narrow transition height range between 419.1 and 469.9 mm, and a broader range between 508 and 932.2 mm that was used to test repeatability. The drop height, impact velocity, impact energy, and fracture results for each trial are listed in table 1.

FSP testing was conducted on samples 32–40 using 0.22-cal. (~1.1-g) steel (4337H or 4340H) projectiles to impact the tiles. The samples were mounted on a heavy steel frame. Each FSP was launched from a pneumatic launcher at high velocity. A Phantom v7 (Vision Research) high-speed camera was set up at 90° to the FSP path to record the impact on the tile. The target area was illuminated by using a high-intensity halogen lamp for backlighting and a diffuser to spread out the light intensity. The focal length and the f-stop of the camera lens were 70 mm and f/8, respectively. The exposure time was 2 μs at 25,000 frames/s, and the resolution was 256 × 256

Table 1. Full drop tower test parameters and fracture results.

Sample	Drop Height (mm)	Impact Velocity (m/s)	Total Energy (J)	Fracture
1	127.0	1.56	4.57	No
2	203.2	1.98	7.31	No
3	279.4	2.33	10.16	No
4 (A)	355.6	2.58	12.45	No
5	419.1	2.81	14.78	No
6	431.8	2.90	15.66	No
7 (B)	431.8	2.88	15.50	No
8 (C)	431.8	2.87	15.40	Yes
9	431.8	2.86	15.24	Yes
10	438.2	2.92	15.92	No
11	444.5	2.91	15.82	Yes
12	444.5	2.91	15.82	Yes
13	444.5	2.90	15.75	No
14	450.8	2.94	16.19	No
15	457.2	2.97	16.50	Yes
16	457.2	2.96	16.36	Yes
17	469.9	3.01	16.87	Yes
18	469.9	2.99	16.70	Yes
19	508.0	3.14	18.37	Yes
20	508.0	3.11	18.02	Yes
21	591.8	3.38	21.30	Yes
22 (D)	591.8	3.38	21.38	Yes
23	678.18	3.61	24.36	Yes
24	678.18	3.62	24.45	Yes
25 (E)	762.0	3.82	27.24	Yes
26	762.0	3.83	27.37	Yes
27	845.8	4.06	30.78	Yes
28	845.8	4.04	30.51	Yes
29	932.2	4.26	33.91	Yes
30	932.2	4.24	33.62	Yes
31	1016.0	4.46	37.19	Yes

pixels. The camera was used to measure the impact velocity. A schematic of the FSP impact testing setup is shown in figure 1. A total of 16 shots were taken on the set of nine samples at velocities ranging from 157.89 to 523.04 m/s. The corresponding impact energies ranged from 13.71 to 150.46 J. The impact velocity, impact energy, and fracture results for each trial are listed in table 2.

After completing the drop tower and FSP test trials under various conditions, visual inspection was conducted by acquiring digital images of the sample surfaces. Projection DR was performed through the thickness of selected samples using a computed tomography system with a 420 kVP

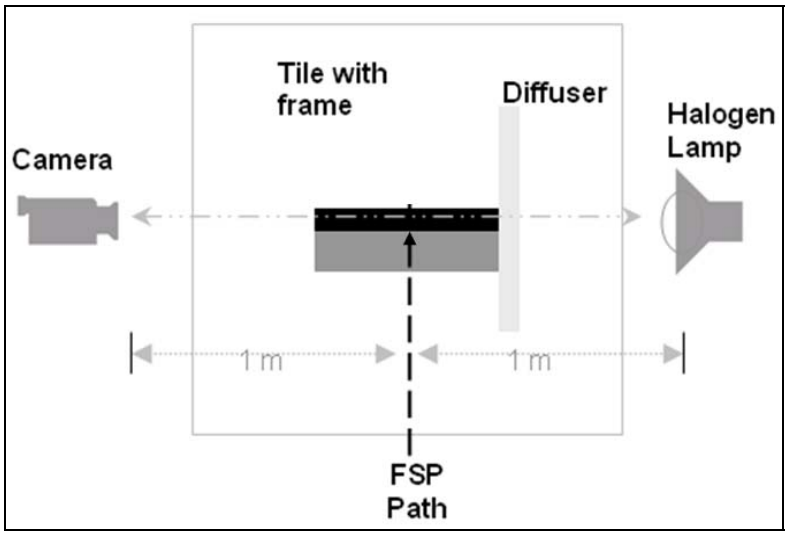

Figure 1. Schematic of FSP testing setup.

Table 2. Full FSP test parameters and fracture results.

Sample	Shot	Impact Velocity (m/s)	Total Energy (J)	Fracture
32 (F)	1	157.89	13.71	No
32 (F)	2	192.02	20.28	No
37	1	213.97	25.18	No
37	2	252.98	35.20	No
33 (G)	1	253.90	35.46	No
32 (F)	3	277.06	42.22	Yes
33 (G)	2	281.03	43.44	No
33 (G)	3	289.86	46.21	Yes
37	3	299.92	49.48	No
40	1	314.86	54.53	Yes
39	1	321.87	56.98	Yes
38	1	335.89	62.05	Yes
37	4	346.86	66.17	Yes
36	1	346.86	66.17	Yes
35 (I)	1	420.01	97.03	Yes
34 (H)	1	523.04	150.46	Yes

x-ray source and a 512 element linear detector array. The tube energy and current used were 400 keV and 2.0 mA, respectively, and the focal spot was 0.80 mm. The source-to-image distance and source-to-object distance were 940 and 750 mm, respectively. UT testing was conducted using a 15-MHz longitudinal transducer with a water immersion testing setup. The reflected signal amplitude values from the bottom surfaces of each Al_2O_3 ceramic were measured to produce C-scan image maps through the bulk of selected samples.

3. Drop Tower Testing Results

After completing drop tower testing on samples 1–31, the data was collected (table 1) and analyzed for further evaluation. The data indicated that a transition from nonfractured to fractured samples occurred at an approximate range of 15.24 to 16.19 J, which corresponded to drop heights between 431.8 and 450.8 mm. This is graphically depicted in figure 2, in which the impact velocities are plotted against the impact energies. In this graph, the blue symbols represent nonfractured samples, and the red symbols represent fractured samples. The circled threshold region in the figure, containing both fractured and nonfractured samples, indicates that no samples tested at impact velocities below 2.86 m/s were fractured, and all samples tested at impact velocities above 2.94 m/s were fractured. While the high-strength steel indenter did not deform during the impact event, higher-impact energy resulted in higher rebound. In the fractured samples, the surface cracks produced by indenter impact were wide enough to make them easily visible. These cracks appeared to penetrate through the thickness of the samples and extend out to the edges. The indenter also produced a cratered impact region in the fractured samples. With increasing impact energy, the number of surface cracks and the size of the impact craters appeared to increase.

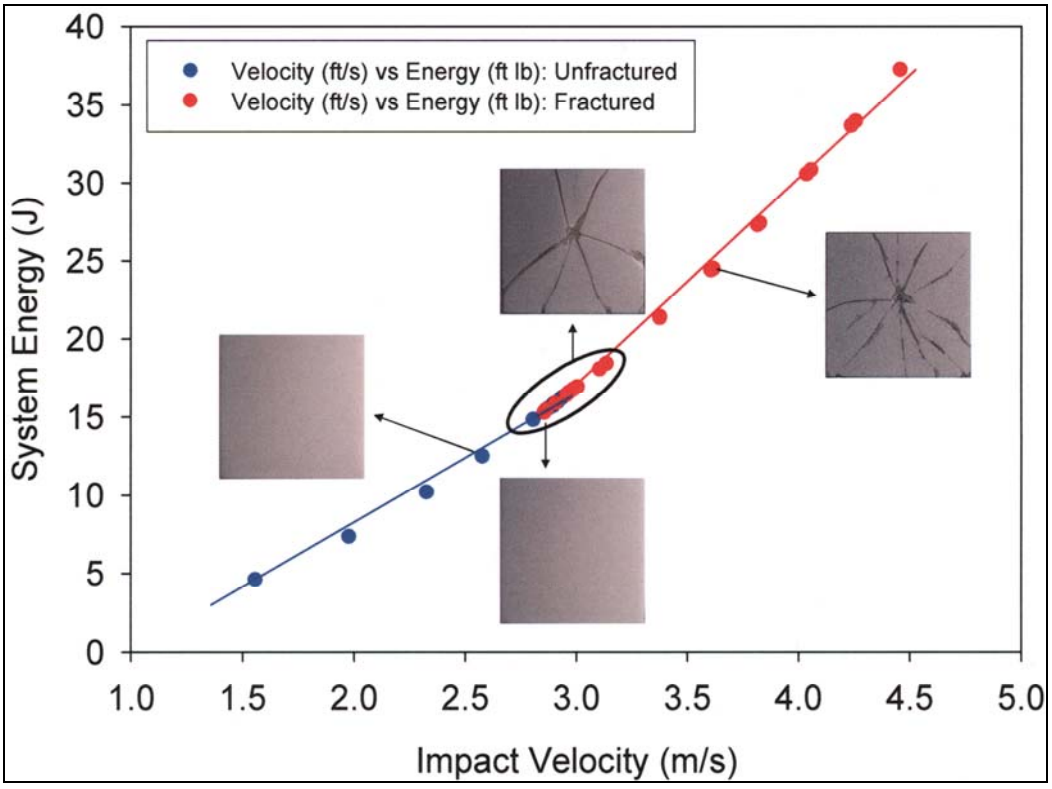

Figure 2. Relationship between impact velocity and initial energy during drop tower testing.

A more detailed description of drop tower testing for samples A, B, C, D, and E (table 1), which were selected for further NDE, is provided. While there was a small mark on sample A (tested at 355.6 mm) where the high-strength steel indenter impacted the sample surface, there were no signs of cracking. As in the general sample trends, drop tower testing at heights above 431.8 mm fractured samples D and E, which were tested at 591.8 and 762.0 mm, respectively. However, the test conditions for samples B and C, which were both tested at a drop height of 431.8 mm, fell within the threshold region, as shown in figure 2. Within this threshold region, approximately half of the samples fractured while the other half did not. This trend was consistent for samples B and C, as sample C fractured while sample B did not. The impact velocities and impact energies varied slightly for sample B at 2.88 m/s and 15.50 J when compared to sample C at 2.87 m/s and 15.40 J.

Digital surface images of samples A, B, C, D, and E were acquired for visual inspection, as shown in figure 3. Samples A and B showed small marks where impact occurred but did not cause fracture, while samples C, D, and E showed fracture origins and resulting crack patterns in the impact regions.

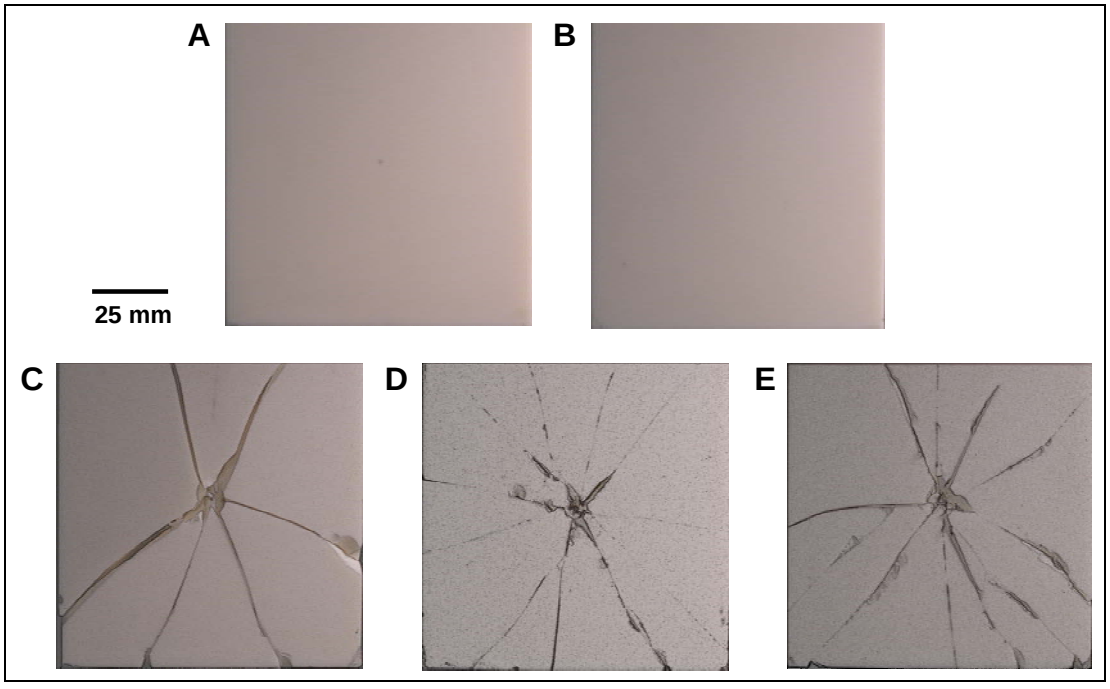

Figure 3. Digital imaging of drop-tower-tested samples for visual inspection.

4. FSP Testing Results

After completing FSP testing on samples 32–40, the data was collected (table 2) and analyzed for further evaluation. The data indicated that a transition from nonfractured to fractured samples occurred in an approximate range of 40.67 to 54.23 J. This is graphically depicted in figure 4, in which the impact velocities are plotted against the impact energies. In this graph, the blue symbols represent nonfractured samples, and the red symbols represent fractured samples. The circled threshold region in the figure, containing both fractured and nonfractured samples, indicates that no samples tested at impact velocities below 274.32 m/s were fractured, and all samples tested at impact velocities above 281.94 m/s were fractured. The projectiles deformed and rebounded in every sample test without penetrating the samples. In the fractured samples, all of the cracks appeared to be very narrow hairline cracks. As opposed to the wider cracks from drop tower testing, the tighter cracks from FSP testing were more difficult to see and did not stand out without the use of appropriate lighting and viewing angle. The majority of cracks appeared to extend through the thickness of the samples to the edges of the ceramic. The number of cracks also appeared to increase with impact energy.

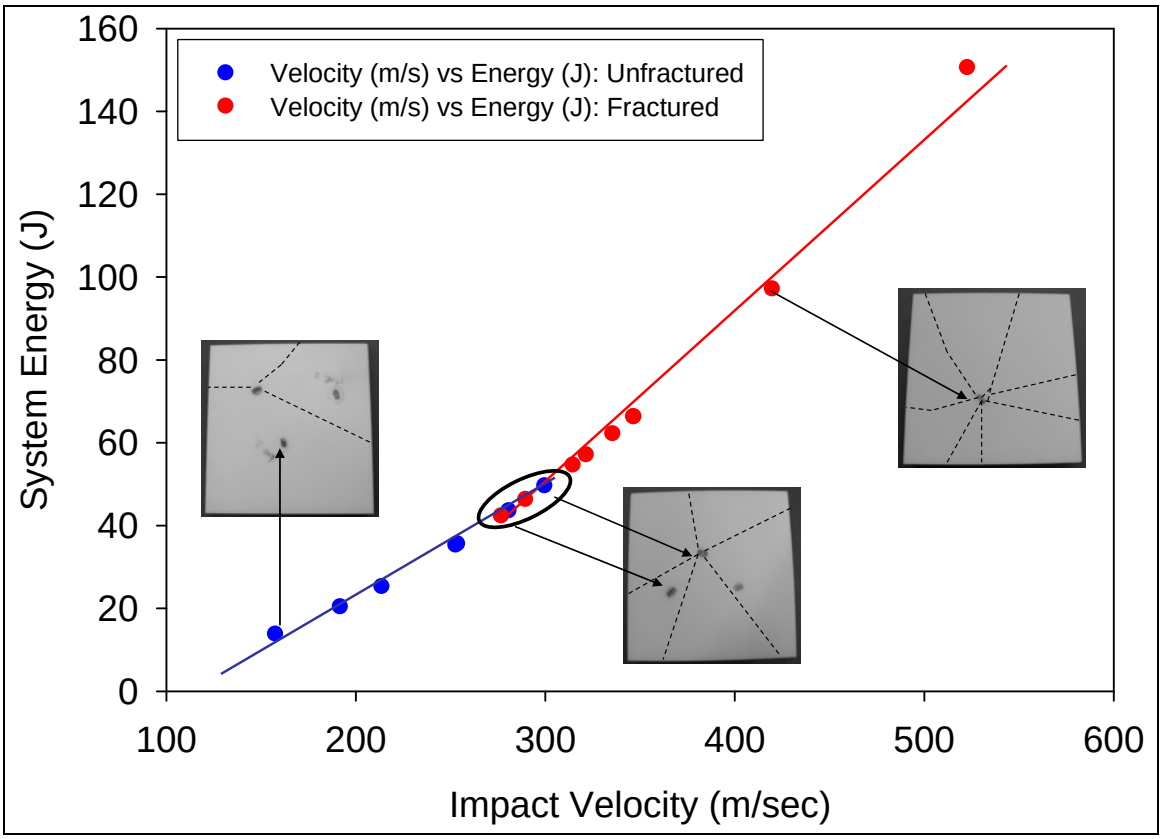

Figure 4. Relationship between impact velocity and initial energy during FSP testing.

A more detailed description of drop tower testing for samples F, G, H, and I (table 2), which were selected for further NDE, is provided. Sample F underwent three FSP trials at three different locations until the surface was visibly damaged. The first two tests on sample F showed no indication of cracking, with an impact velocity of 157.89 m/s and impact energy of 13.71 J for shot 1 and an impact velocity of 192.02 m/s and impact energy of 20.28 J for shot 2. For shot 3, the impact velocity was increased to 277.06 m/s and impact energy to 42.22 J, and the result was visible hairline cracking from the point of FSP impact. Similarly, sample G underwent three FSP trials at different locations. The velocities were chosen to determine a specific threshold range. Again, the first two FSP tests on sample G showed no indication of cracking, with an impact velocity of 253.90 m/s and impact energy of 35.46 J for shot 1 and an impact velocity of 281.03 m/s and impact energy of 43.44 J for shot 2. While it was expected that fracture should occur above 277.06 m/s based on the results from sample F, it was not until the third shot with an impact velocity of 289.86 m/s and impact energy of 46.21 J that fracture occurred. This indicated an impact velocity threshold range for the FSP tests rather than a specific threshold value. The next two FSP tests for samples H and I were conducted at significantly higher impact velocity and impact energy values of 523.04 m/s and 150.46 J for sample H and 420.01 m/s and 97.03 J for sample I, respectively. As expected, both of these tests resulted in fracture and hairline cracking in the alumina samples.

Digital surface images of samples F through I were acquired for visual inspection, as shown in figure 5. Since the hairline cracks were difficult to see in the photographic reproductions, dotted lines were drawn over the surface crack patterns. Impacts from the first two shots on samples F and G showed marks where impact occurred but did not cause fracture. Impacts from the third shot on sample F, the third shot on sample G, sample H, and sample I showed fracture origins and resulting crack patterns.

5. Digital Radiography Imaging

5.1 Drop Tower Test Samples

X-ray DR was conducted on representative samples A through E, as shown in figure 6, for damage assessment and comparison to visual inspection. The 2-D bulk imaging data collected through the thickness of each sample showed crack patterns that were consistent with visual inspection. Several additional features were also detected that were not picked up by visually inspecting the sample surfaces. Darker features in the DR images corresponded to a higher degree of x-ray attenuation and more pronounced damage. The largest cracks showed up as the darkest features in contrast to lighter, undamaged regions.

The DR images for samples A and B, which were dropped from the lowest heights of 355.6 and 431.8 mm, respectively, and did not fracture, appeared to be homogeneous, with no distinct

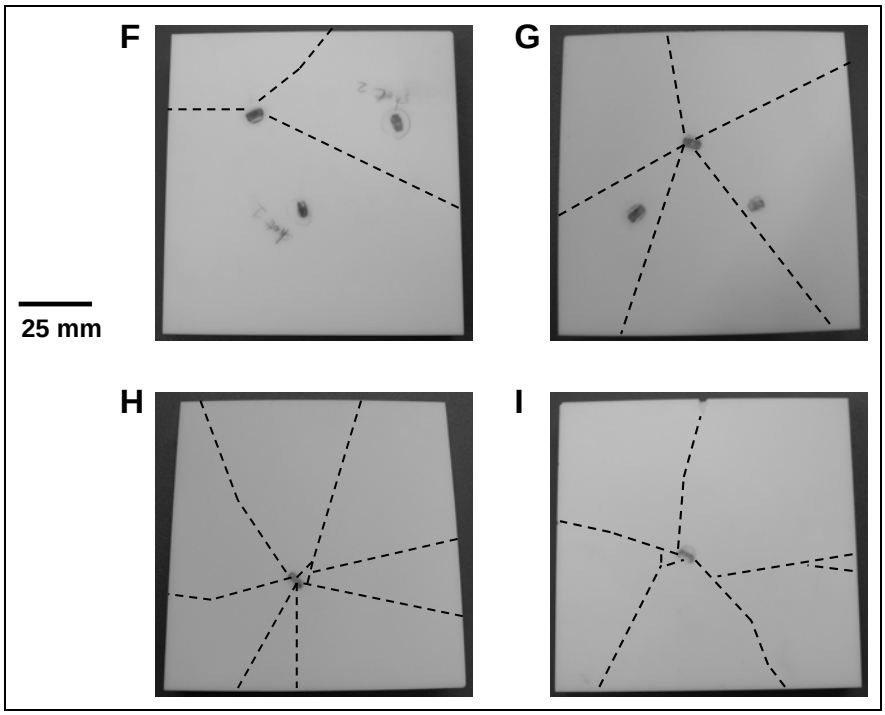

Figure 5. Digital imaging of FSP-tested samples for visual inspection.

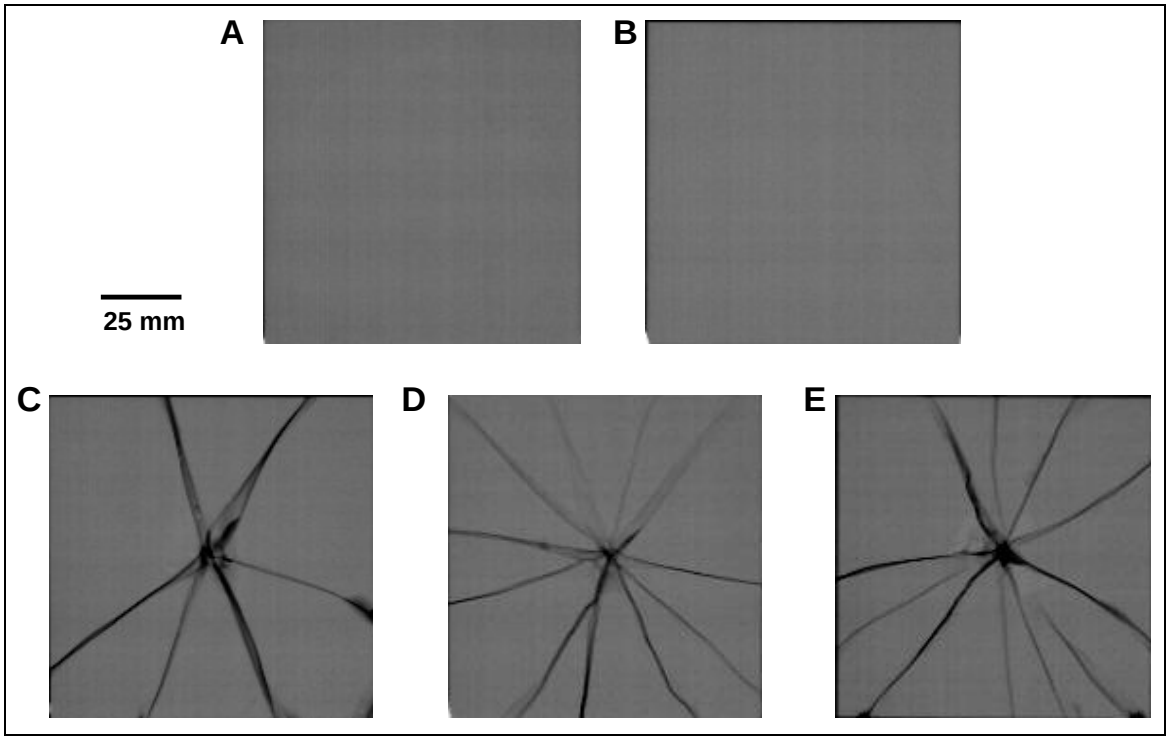

Figure 6. X-ray DR of drop-tower-tested samples for NDE.

features that could be readily detected. The point impact regions in which the indenter contacted the alumina samples did not have a high enough x-ray attenuation to be resolved. Sample C, which was dropped from 431.8 mm and did fracture, showed the six major cracks that originated from the impact area and extended to the sample edges. Some of the cracks, such as the left crack extending to the top surface and the right crack extending to the bottom surface, appeared to be wider since they were imaged through the full thickness of the sample. The DR image of sample D, which was dropped from 591.8 mm, showed eleven major cracks that extended from the impact area to the edge of the sample. Two additional cracks with slight attenuation differences, compared to the undamaged material, were also found, one extending from the major crack in the bottom left corner, and another connecting two cracks in the upper left corner. All of the cracks in the bottom half of the sample also appeared to be much darker than the cracks in the upper half of the sample, suggesting that their crack widths were larger through the sample volume. Sample E, which underwent the highest indenter drop height of 762 mm, also showed 11 major cracks in the DR image. In addition, several other features exhibiting x-ray attenuation were noted, including a circular feature in contact with one of the major cracks, a small crack extending to the lower right corner of the sample, and an isolated edge crack near the bottom right corner. While DR imaging was able to detect all of the major cracks that were visible on the sample surface, only minor variations attributed to bulk specimen damage were found.

For quantitative damage comparison, the percent area from darker regions of the DR images was assessed to estimate the degree of damage in each of the five representative samples. The calculated values were 0.00% for A, 0.00% for B, 14.06% for C, 14.22% for D, and 23.37% for E, as shown in table 3. While no damage was found in samples A and B, the percent damage values for samples C, D, and E increased with drop height, impact velocity, and impact energy.

Table 3. Selected drop tower test parameters and quantitative damage results.

Sample	Drop Height (mm)	Impact Velocity (m/s)	System Energy (J)	Fracture	DR Damage (%)	UT Damage (%)
A	355.6	2.58	12.45	No	0.00	0.17
B	431.8	2.88	15.50	No	0.00	0.18
C	431.8	2.87	15.40	Yes	14.06	23.73
D	591.8	3.38	21.38	Yes	14.22	28.85
E	762.0	3.82	27.24	Yes	23.37	36.33

5.2 FSP Test Samples

DR was performed on samples F through I, as shown in figure 7, to compare the detected damage to visual inspection. Again, the image data collected through each sample thickness showed crack patterns and damage that was consistent with what was detected visually. Since the hairline cracks could not be imaged well through visual inspection, the dotted line patterns

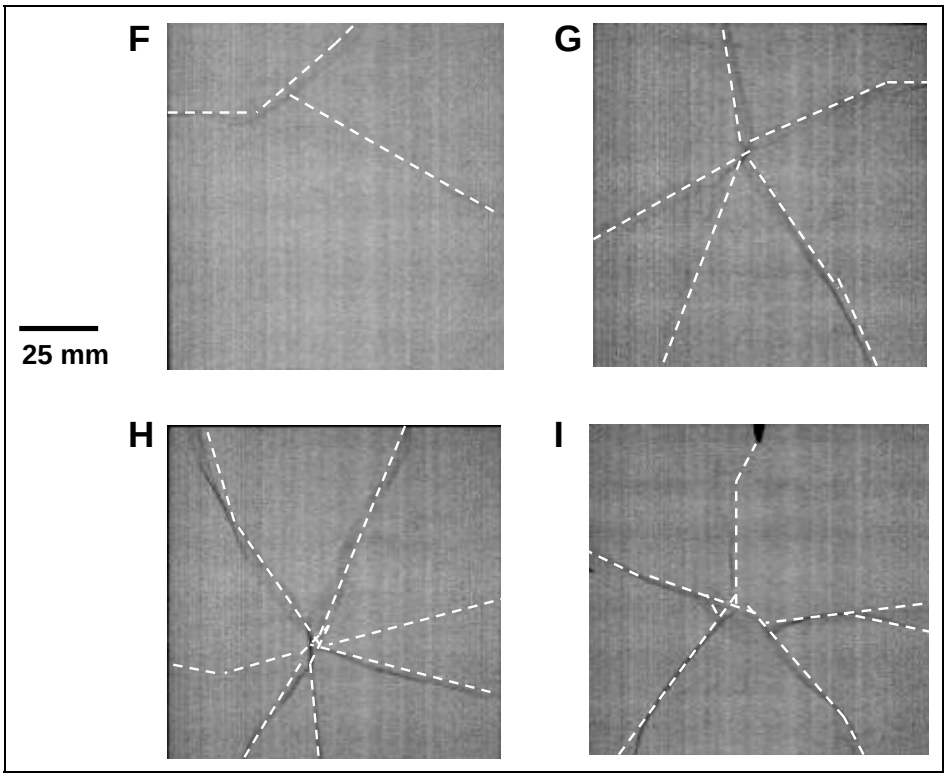

Figure 7. X-ray DR of FSP-tested samples for NDE.

were used as a guideline for visual comparison. In the DR images, the dark features indicated higher x-ray attenuation and represented the most prominent cracks. These damaged regions were contrasted against the lighter background of the undamaged alumina regions. The darkest cracks demonstrated the largest widths and the highest degrees of damage.

While surface cracks were detected using DR, the contrast of some of these hairline cracks was not very high due to the narrow crack widths. Some of these hairline cracks were barely visible in the DR images while others stood out clearly. For sample F, no indication of damage was detected for the first two shots, but three surface cracks caused by the third shot were found. While the cracks extending to the upper and left edges of the sample were prominent, the crack extending to the right edge was much fainter in the DR image, despite optimization of the contrast. For sample G, the impact locations for the first two FSP shots showed no sign of damage. However, all five of the surface cracks detected from the third shot during visual inspection were found in the DR image. For sample H, five of the seven hairline cracks observed from visual inspection were detected. Two of the cracks extending through the point of impact, one to the left edge of the sample, and the other to the upper right edge of the sample could not be contrasted. The crack widths were too narrow to be detected by DR. However, there were some features detected in the DR images that could not be found by visually observing the surface of sample H. Upon close inspection, intricate crack patterns of multiple

cracks overlapping each other were found. Wider damage bands around the cracks were also detected. For sample I, the five cracks that were found during visual inspection were also detected in the DR image. The crack extending to the upper edge was very faint compared to the other four cracks. However, there were also features in the DR image that were not found when examining the sample visually, including a small crack that partially extended from the point of impact and a crack near the point of impact connecting two of the major cracks. Overall, while a few of the hairline cracks were not detected in the DR images, the image details for those that were detected resulted in improved damage detection.

For quantitative damage comparison, the images were inverted and converted to grayscale, with the dark regions representing areas in which damage occurred, as shown in figure 7. The values for sample F were 0.00% for shot 1, 0.00% for shot 2, and 1.81% for shot 3. The values for sample G were 0.00% for shot 1, 0.00% for shot 2, and 5.05% for shot 3. The values for samples H and I were 6.13% and 7.15%, respectively, as shown in table 4.

Table 4. Selected drop tower test parameters and quantitative damage results.

Sample	Shot	Impact Velocity (m/s)	System Energy (J)	Fracture	DR Damage (%)	UT Damage (%)
F	1	157.89	13.71	No	0.00	0.00
F	2	192.02	20.28	No	0.00	0.09
F	3	277.06	42.22	Yes	1.81	13.23
G	1	253.90	35.46	No	0.00	0.00
G	2	281.03	43.44	No	0.00	0.11
G	3	289.86	46.21	Yes	5.05	14.10
I	1	420.01	97.03	Yes	7.15	19.56
H	1	523.04	150.46	Yes	6.13	19.11

6. Ultrasound C-Scan Imaging

6.1 Drop Tower Test Samples

UT C-scan imaging was conducted on samples A through E for damage assessment and comparison to visual inspection. Selecting the alumina bottom surface signal for amplitude evaluation enabled bulk characterization of the tile without interference from the aluminum backing plate. The color scale was set up in terms of attenuation, or signal loss, in decibels (dB), with red representing the highest degree of signal loss, green representing a medium signal loss, and blue representing the lowest degree of signal loss.

UT C-scan images are shown in figure 8. The image for sample A showed a circular region in the center of the sample with a significant level of signal loss compared to the surrounding areas. This region was at the point of impact and was considered to be the only source of damage to the sample, as no cracking was detected. Material variations in the sintered alumina that were not a

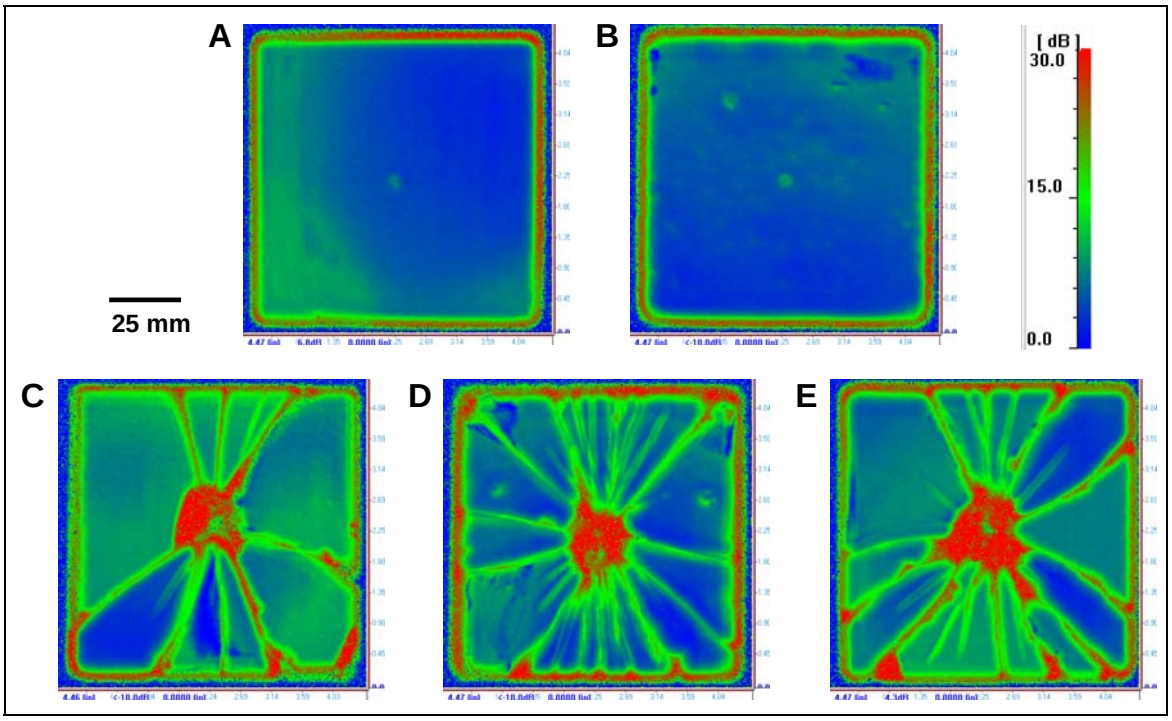

Figure 8. UT C-scan imaging of drop-tower-tested samples for NDE.

result of low-velocity impact were also detected by the longitudinal 15-MHz transducer. A region along the left side of the sample with a higher level of attenuation indicated a slightly lower density compared to the rest of the sample. The C-scan image for sample B also showed a circular region in the center of the sample with significant signal loss. This region was slightly larger in area and higher in attenuation as compared to the region in sample A. Other features that were detected in the scan were three surface defects in the upper half of the sample and some minor density variations in the upper right hand corner of the sample.

While there was no crack damage detected for samples A and B, UT C-scan images of samples C, D, and E demonstrated significant impact damage and crack patterns. The regions with the highest degree of attenuation were most evident for the largest cracks and at the point of impact. Sample C, which was tested at a drop height of 431.8 mm, showed eight cracks that extended from the impact region to the edge of the sample. Three additional cracks were also identified, including one that originated from a major crack and extended to the upper edge, one that started from the impact area and extended halfway toward the bottom left corner, and one that extended straight down to the bottom edge. All of these cracks exhibited a lower degree of attenuation compared to the eight main cracks. Regional material variations were also present, as the bottom left corner showed lower signal loss than the rest of the sample. Sample D, which was tested at a drop height of 591.8 mm, appeared to have an impact region similar in area to sample C but showed more cracking throughout the sample. Fourteen cracks extended from the impact region to the edge of the sample. Five cracks originated at the impact region without extending to the edge. There were also four additional cracks that extended from the major cracks. Surface

damage and density variations not caused by impact were also detected in sample D. Sample E, which was dropped from a height of 762.0 mm, had the largest impact area, which was roughly twice as large as those in samples C and D. There were 12 cracks that extended from the impact area to the sample edge, two cracks that originated from main cracks, and five that did not reach the edge. Qualitatively, while the number of cracks did not directly correspond to the drop height, the highest-velocity, highest-energy impact from 762.0 mm produced the largest impact area.

For quantitative damage comparison, the images were inverted and converted to grayscale, with the dark regions representing areas in which damage occurred, as shown in figure 9. The values for the representative samples were 0.17% for A, 0.18% for B, 23.73% for C, 28.85% for D, and 36.33% for E, as shown in table 3. The degree of quantitative damage increased with drop height for the five samples. As compared to the DR images, the damage percentages were higher in the UT images due to additional damage detected in the bulk. The percent damage also increased incrementally for the three fractured samples.

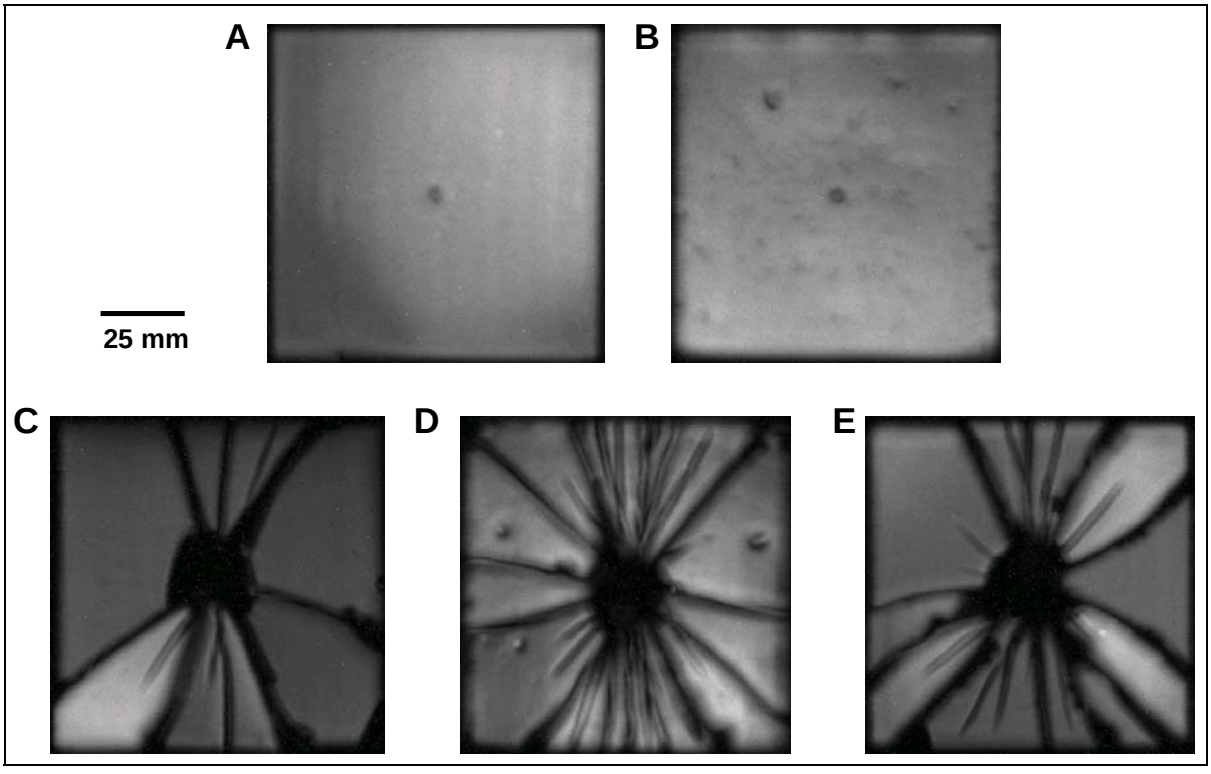

Figure 9. Grayscale drop tower C-scan imaging for quantitative damage assessment.

6.2 FSP Test Samples

UT C-scan imaging was conducted on samples F through I to assess damage and compare to visual inspection. Again, variations in the alumina bottom surface signal were used to evaluate bulk sample damage. The same color scale was utilized to determine the degree of attenuation, with red representing the highest degree of signal loss.

The C-scan images are shown in figure 10. For sample F, damage assessment was evaluated individually for each of the three shots. The location of shot 1 at 157.89 m/s showed no increase in attenuation at the point where the projectile contacted the sample. However, the impact location for shot 2 at 192.02 m/s did show a small region with a higher degree of attenuation. This point of impact from shot 2 was isolated from any other damage identified in the rest of the sample and was not believed to have influenced the degree of damage caused by the third shot. The C-scan image of shot 3 at 277.06 m/s showed significant damage, with four major cracks extending from the point of impact. Three of these major cracks extended from the impact point to the sample edge, and two smaller additional cracks originating from the major cracks were also identified. One region in the bottom left corner with a higher degree of attenuation indicated a lower density compared to the rest of the sample. For sample G, the damage assessment was evaluated separately for each of the three shots. The location of impact for shot 1 showed no attenuation variation. It was expected that there should be some change since the velocity of the FSP for this test was 253.90 m/s, but no damage was detected. The impact location for shot 2 at 281.03 m/s showed a small area of isolated damage, with no sign of cracking or additional damage extending from it. The impact location of shot 3 at 289.86 m/s showed five major cracks extending from the origin, all of which propagated to the edge of the alumina sample. Other detectable features were a small crack extending from one of the major cracks and a highly attenuated region in the upper right corner that appeared to be a defect and was unrelated to the FSP tests.

As opposed to samples F and G, which required three FSP tests each to create extensive damage, samples H and I each produced significant cracking damage after one test. For sample I, which was tested at a velocity of 420.01 m/s, the UT C-scan image showed a very large damage region at the point of impact. From this region, six cracks were detected, all of which extended to the sample edge. For sample H, which was tested at the highest FSP velocity of 523.04 m/s, the C-scan image showed significant damage at the point of impact. While the extent of damage at the point of impact was not as large as for sample I, there were more cracks that originated from the impact location. Eight cracks, all of which extended to the sample edge, were detected in sample H as opposed to six from sample I. Of the four FSP tests that caused significant damage to the alumina samples, UT C-scan imaging showed that the number of cracks originating from the point of impact increased with the velocity and energy of the test. While sample F showed four cracks at 277.06 m/s and 42.22 J, sample G showed five cracks at 289.86 m/s and 46.21 J,

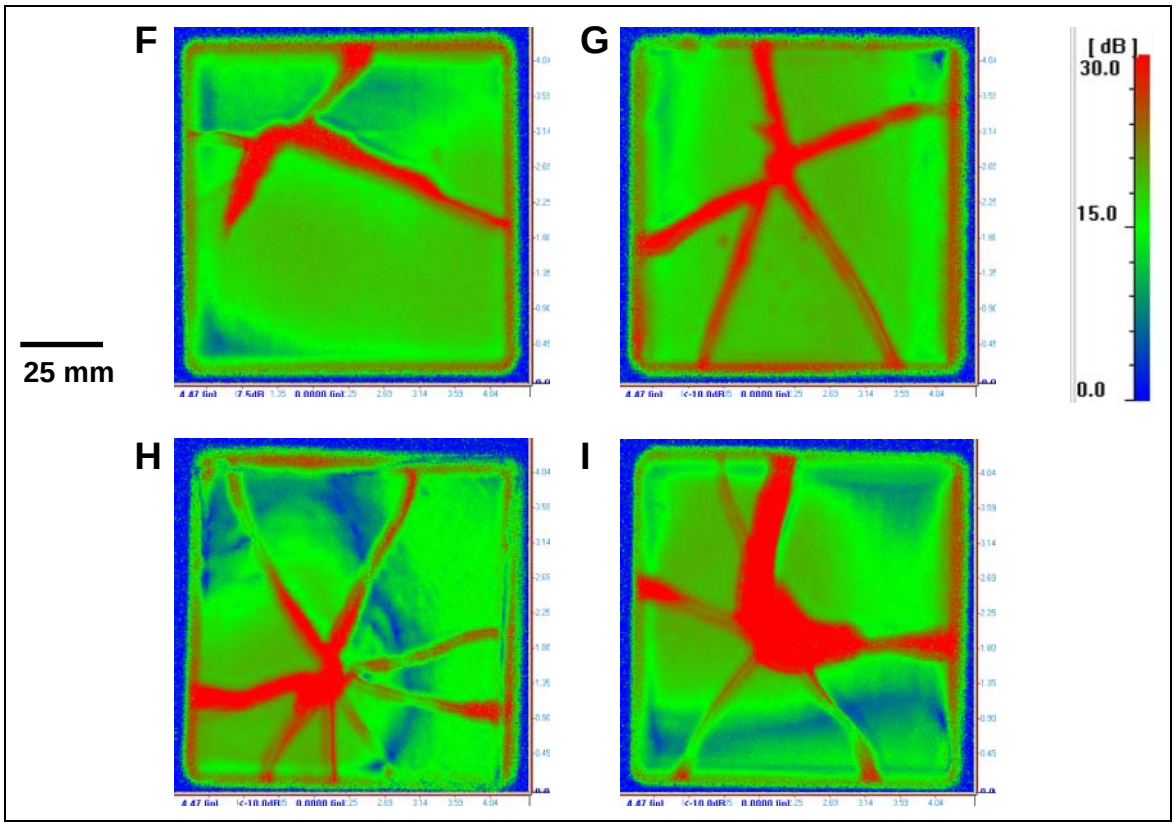

Figure 10. UT C-scan imaging of FSP-tested samples for NDE.

sample I showed six cracks at 420.01 m/s and 97.03 J, and sample H showed eight cracks at 523.04 m/s and 150.46 J.

For quantitative damage comparison, the images were inverted and converted to grayscale, with the dark regions representing areas in which damage occurred, as shown in figure 11. The values for sample F were 0.00% for shot 1, 0.09% for shot 2, and 13.23% for shot 3. The values for sample G were 0.00% for shot 1, 0.11% for shot 2, and 14.10% for shot 3. The value for sample H was 19.11% and 19.56% for sample I, as shown in table 4. The percent damage in the four fractured samples increased before leveling off at the two highest velocities. UT C-scan imaging proved to be an effective technique for characterizing and quantifying damage in the alumina samples.

7. Comparison of NDE Methods and Visual Inspection

Comparison of visual inspection to UT and DR demonstrated the capabilities of NDE methods for detecting internal bulk damage in the Al_2O_3 samples, as shown in figures 12–20. Both techniques successfully identified the largest cracks, which added up to 6 for sample C, 11 for sample D, 11 for sample E, 4 for sample F, 5 for sample G, 6 for sample I, and 8 for sample H.

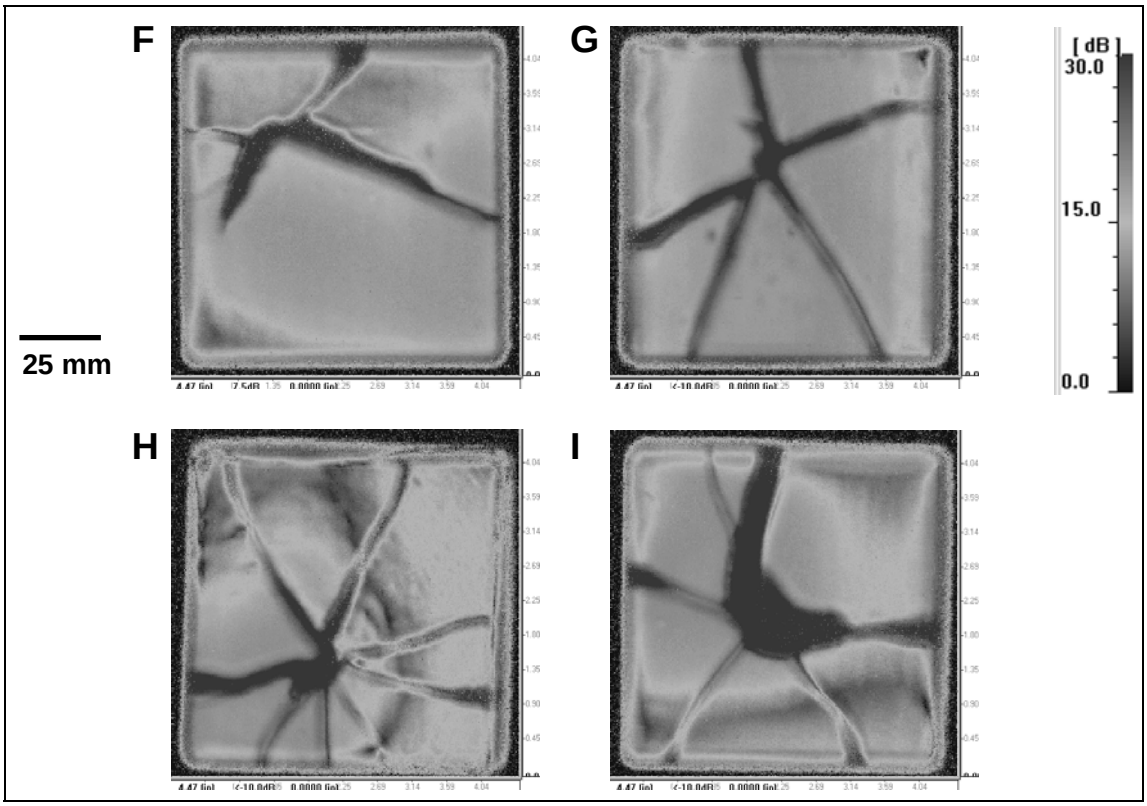

Figure 11. Grayscale FSP test C-scan imaging for quantitative damage assessment.

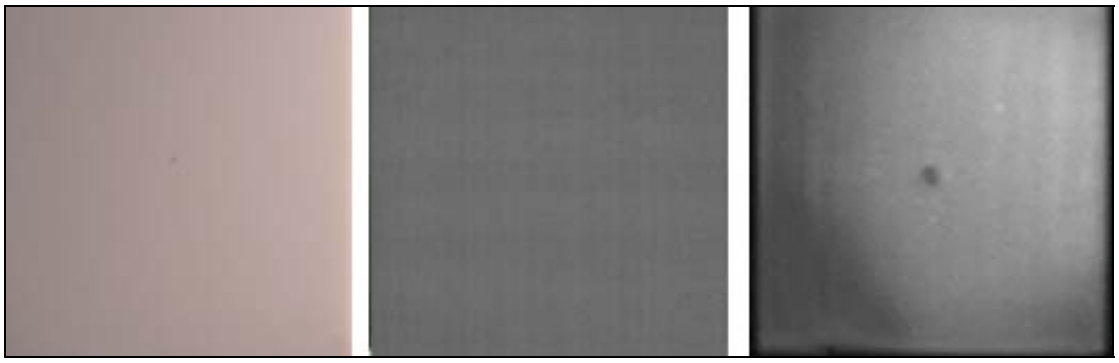

Figure 12. Comparison of visual inspection (left), DR (center), and UT (right) for sample A.

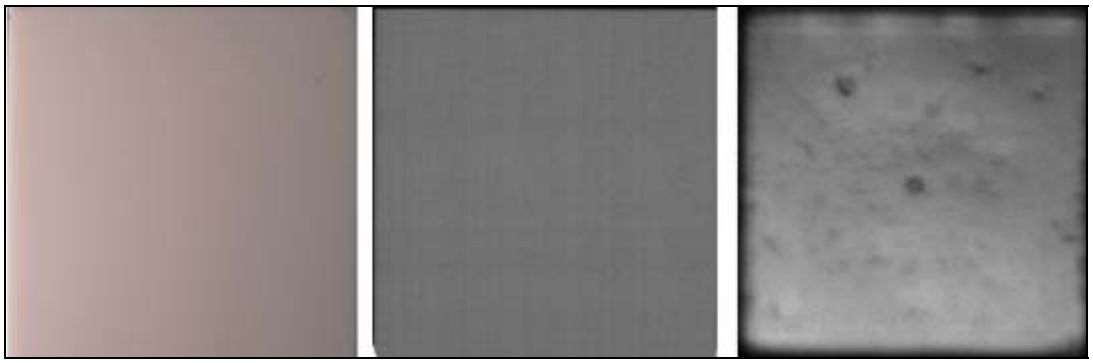

Figure 13. Comparison of visual inspection (left), DR (center), and UT (right) for sample B.

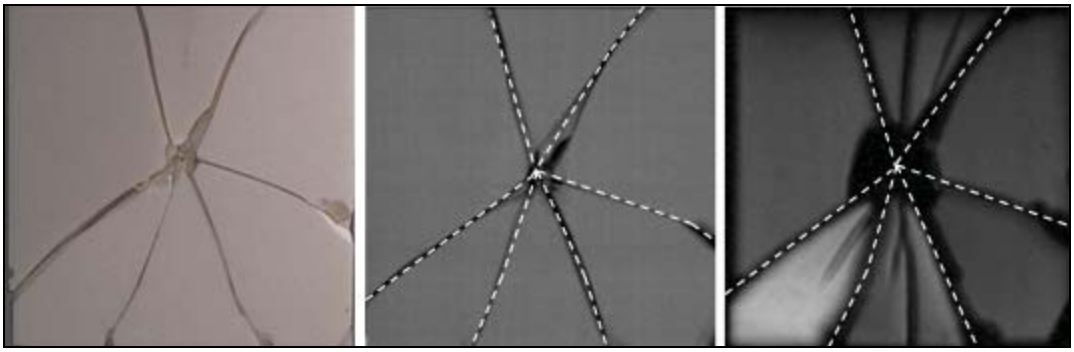

Figure 14. Comparison of visual inspection (left), DR (center), and UT (right) for sample C.

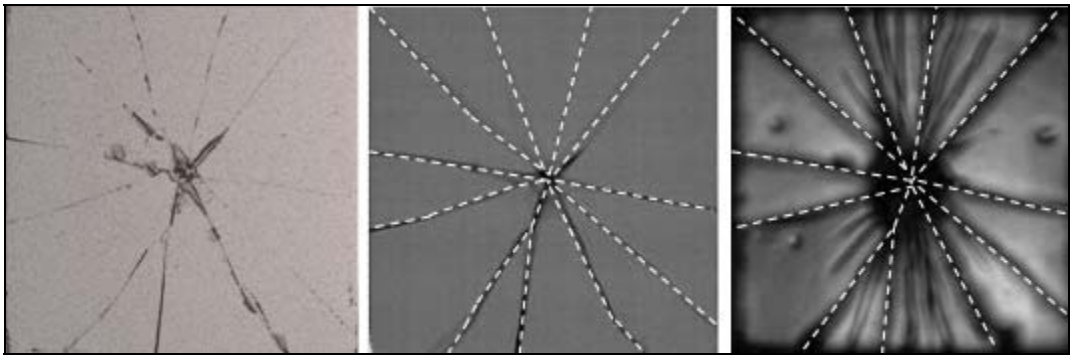

Figure 15. Comparison of visual inspection (left), DR (center), and UT (right) for sample D.

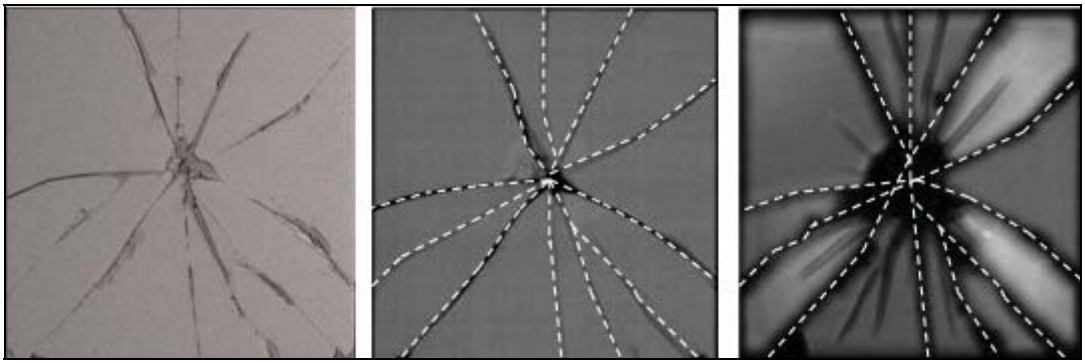

Figure 16. Comparison of visual inspection (left), DR (center), and UT (right) for sample E.

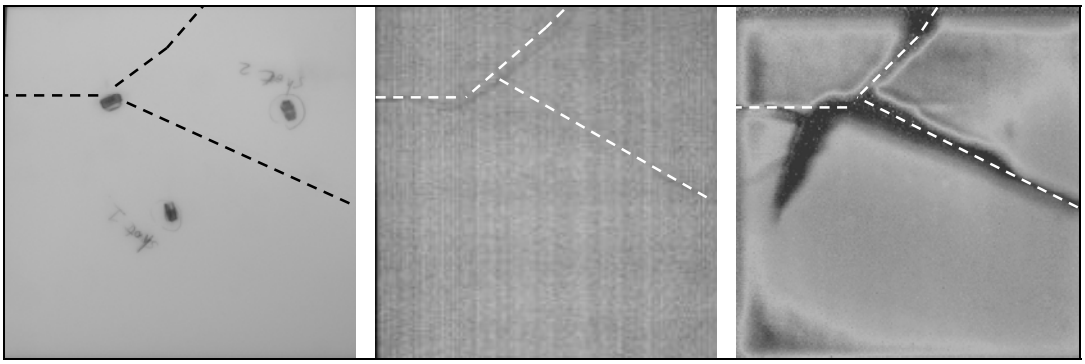

Figure 17. Comparison of visual inspection (left), DR (center), and UT (right) for sample F.

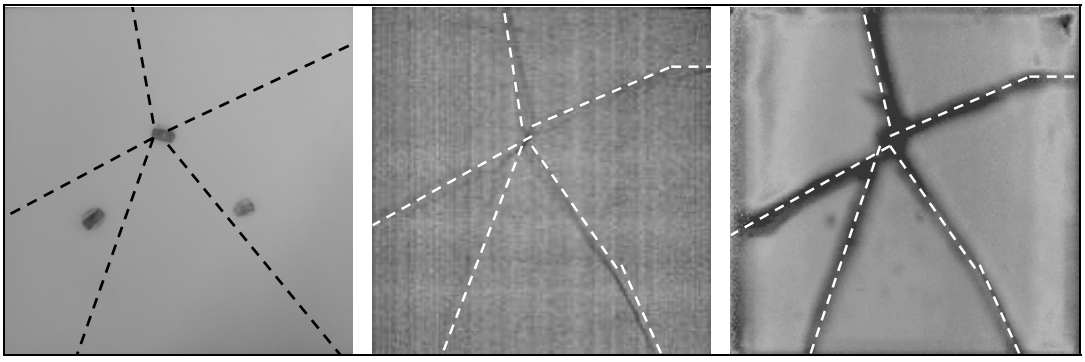

Figure 18. Comparison of visual inspection (left), DR (center), and UT (right) for sample G.

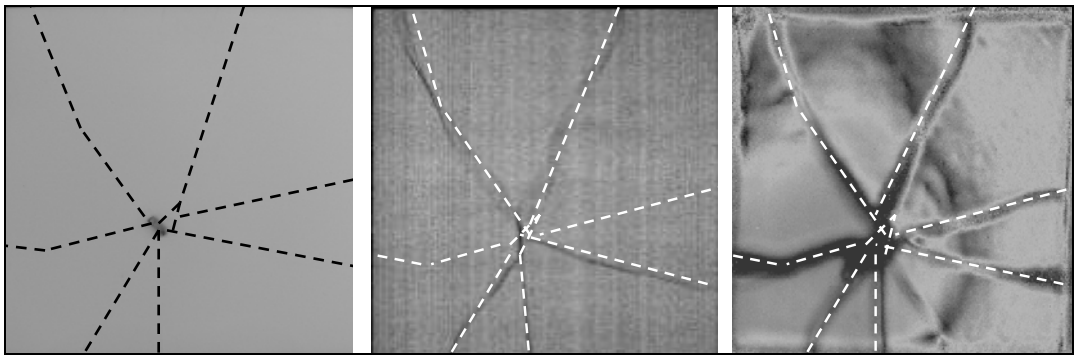

Figure 19. Comparison of visual inspection (left), DR (center), and UT (right) for sample H.

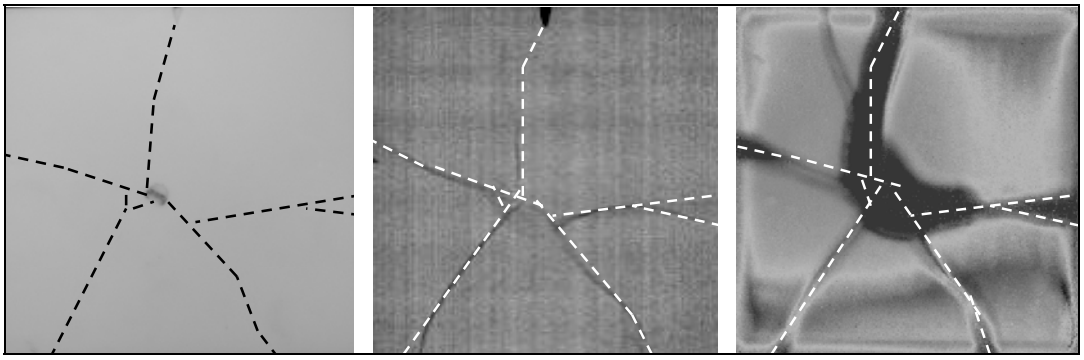

Figure 20. Comparison of visual inspection (left), DR (center), and UT (right) for sample I.

The DR images demonstrated the crack widths through the bulk of each sample, which often appeared wider in the images than they did during visual inspection. The intricate overlapping crack patterns in the samples were also identified much more clearly using DR as opposed to simple visual inspection. For the FSP samples, this was even more crucial since the damage identified on the surface was caused by hairline cracks, which were very difficult to detect. Dotted lines were used to identify these hairline crack locations due to this limitation. Some small cracks and flaws that could not be detected by visual inspection were also identified by the DR method. However, it was not until a UT evaluation was conducted that the full extent of bulk damage was uncovered.

In addition to detecting all the major cracks found by both visual inspection and DR, a large degree of bulk damage was detected during C-scan imaging. This damage, while consistent with the types of crack patterns on the surface, was not detected on the exterior of the samples. This damage was believed to be the result of internal cracks that were present in the bulk of the samples. The number of significant internal cracks found by C-scan imaging of the drop-tower-tested samples was 5 in sample C, 12 in sample D, and 8 in sample E. The number of significant internal cracks found by C-scan imaging of the FSP-tested samples was three for sample F, one for sample G, one for sample H, and one for sample I. While the number of internal cracks was higher for the drop-tower-tested samples than the FSP-tested samples, all of the internal cracks

that were identified represented damage that would not have been accounted for if visual inspection or DR testing were used alone. By identifying the extended bulk damage in the samples, more accurate quantitative damage values were obtained. Besides the characterization of internal damage in the samples, material variations were also detected. For samples A, B, and F, minor impact damage was detected by C-scan imaging that was not found using the other methods. In addition, minor density variations that were not detected through visual inspection or DR imaging were found in every UT C-scan image. This was most evident in samples A and B in which the DR images appeared completely homogeneous.

A full inspection of drop-tower-tested sample C, as shown in figure 14, will be detailed from initial visual inspection through DR and UT C-scan imaging. The visual inspection of sample C was straightforward since the exterior cracks were wide. The six cracks extending from the point of impact were clearly evident. After DR was conducted, the resulting image was very similar to the external snapshot acquired during the visual inspection. The large widths of the six cracks were well within the detectable resolution limits of the technique and showed up very well in the digital radiograph. There were also some details detected by DR that were not evident by visually observing the sample exterior. While it appeared that there was a single wide region of damage near the point of impact extending to the upper right corner of the sample, the digital radiograph through the sample bulk indicated otherwise. In addition to a significantly large damage region, the radiograph showed two individual cracks that originated from the point of impact and combined to form a single crack before extending to the edge of the sample. This detail signified the advantage of using DR to look through the sample for signs of damage that were not apparent on the surface. After UT C-scan imaging was conducted, the resulting image showed a much higher degree of damage through the sample due to a higher sensitivity compared to DR. The damage region at the point of impact was much larger, extending farther into the sample and overshadowing the crack detail that was found in the digital radiograph. There were also four internal cracks, three of which extended to the edge of the sample, that were detected in regions where there was no indication of damage in either the visual snapshot or the digital radiograph. The crack extending to the bottom edge of the sample split into two distinct cracks, one which propagated to the sample edge. These image details revealed damage that would have otherwise gone undetected and showcased the comparative detection capabilities of UT C-scan imaging over the other methods.

The detection differences between the two NDE techniques were due to the nature of inspection. While the DR method detected bulk features based on x-ray attenuation, the UT method detected bulk features based on acoustic impedance mismatch and acoustic signal attenuation. For the DR images, the internal cracks that could not be detected had widths that were smaller than the x-ray spatial resolution. These were hairline fractures or kissing cracks with narrow gap sizes that were averaged out while collecting the x-ray data. On the other hand, the C-scan images were very sensitive to acoustic impedance mismatch between the alumina tile and the immersion medium. Due to this large mismatch, the bottom surface reflected signal amplitude from the

ceramic tile was reduced, resulting in a corresponding increase in attenuation. These variations were identified by the 15-MHz longitudinal transducer during C-scan imaging of the samples. This inherent detection characteristic proved to be the difference during detection of internal damage. For this application, UT NDE was the better choice for full characterization and quantification of bulk damage caused by fracture of the Al_2O_3 samples.

8. Comparison of Drop Tower Testing and FSP Testing

Several similarities and differences were found between drop tower test results conducted at low velocity/high mass and the FSP testing results conducted at high velocity/low mass. The main similarity was the presence of a threshold range below which the sample did not fracture and above which the sample experienced fracture. Despite the use of the same set of test samples, the conditions of each test method caused these threshold ranges to be drastically different. For the drop-tower-tested samples, the threshold range fell between 15.33 and 15.66 J. For the FSP-tested samples, the threshold range fell between 41.39 and 43.73 J. Qualitatively, the number of surface cracks tended to be higher for the drop-tower-tested samples, with 8 for sample C, 11 for sample D, and 11 for sample E, as opposed to three for sample F, five for sample G, seven for sample H, and five for sample I. The number of internal cracks detected by UT C-scan imaging was also higher for the drop-tower-tested samples, with 5 for sample C, 12 for sample D, and 8 for sample E, as opposed to three for sample F, one for sample G, one for sample H, and one for sample I. For the FSP samples, the damage was concentrated around the point of impact rather than spreading throughout the sample. For the drop-tower-tested samples, the damage appeared to spread throughout the sample, as the average number of surface and internal cracks were higher. Quantitatively, the percent damage in the UT C-scan images was higher for the drop-tower-tested samples. While the damage percentage values were 23.73% for sample C, 28.85% for sample D, and 36.33% for sample E, the values for FSP-tested samples were 13.23% for sample F, 14.10% for sample G, 19.11% for sample H, and 19.56% for sample I. While the drop-tower-tested samples experienced approximately the same incremental percent of damage at higher drop heights, the FSP-tested-sample damage percentages started to level out at the highest velocities. Comparison of both the destructive test methods of drop tower testing and FSP testing and the nondestructive test methods of visual inspection, DR, and UT C-scan imaging showed many important trends. Drop tower testing and UT C-scan imaging appeared to be the most consistent way of identifying qualitative and quantitative damage in Al_2O_3 samples for this study.

9. Conclusions

A combination of quasi-static destructive testing methods for producing incremental damage and nondestructive imaging methods for studying resulting fracture and damage in Al_2O_3 ceramic, aluminum-backed samples was described. Drop tower and FSP testing were both effective for creating damage in the samples. Both methods produced through thickness cracks that extended to the edges of the samples and an increase in the number of cracks with impact energy. The FSP impacts produced very tight hairline cracks while the indenter impacts produced relatively separated and more jagged cracks, as well as cratered impact centers. There was a well-defined transition range and separation between the behavior of nonfractured and fractured samples in terms of the impact energy in both the FSP and drop tower tests. For drop tower testing, a threshold region between 2.87 and 2.90 m/s was determined below which no fracture occurred and above which fracture occurred. For FSP testing, a threshold region between 274.32 and 281.94 m/s was determined below which no fracture occurred and above which fracture occurred.

After collecting digital images of the nine representative samples, nondestructive testing through x-ray DR and UT C-scan imaging was performed. In addition to detecting all of the surface cracks found by visual inspection, DR also detected minor cracking and damage. Quantitative damage percentages for the seven fractured samples were found to be 14.06% for sample C (drop height = 431.8 mm, impact velocity = 2.87 m/s, impact energy = 15.40 J), 14.22% for sample D (drop height = 591.8 mm, impact velocity = 3.38 m/s, impact energy = 21.38 J), 23.37% for sample E (drop height = 762 mm, impact velocity = 3.82 m/s, impact energy = 27.24 J), 13.23% for sample F (impact velocity = 277.06 m/s, impact energy = 42.22 J), 14.10% for sample G (impact velocity = 289.86 m/s, impact energy = 46.21 J), 19.56% for sample I (impact velocity = 420.01 m/s, impact energy = 97.03 J), and 19.11% for sample H (impact velocity = 523.04 m/s, impact energy = 150.46 J).

UT C-scan imaging was a much more effective technique for nondestructively detecting internal damage in the samples, finding a significant number of cracks that were not detected through DR. The number of internal cracks detected was much higher for the drop-tower-tested samples, with 5 for sample C, 12 for sample D, and 8 for sample E, as opposed to three for sample F, one for sample G, one for sample H, and one for sample I. Additional surface damage and material variations were also found through C-scan imaging. The additional bulk damage detected through UT C-scan imaging increased the accuracy of quantitative damage evaluation. Quantitative damage percentages for the fractured samples increased to 23.73% for sample C, 28.85% for sample D, and 36.33% for sample E. Based on these values, the approximate percentage of internal damage detected by UT that could not be detected through DR was 9.67% for sample C, 14.63% for sample D, and 13.29% for sample E. While this study was performed to determine bulk damage characteristics for Al_2O_3, similar studies can be applied to evaluate damage in other opaque materials such as SiC and B_4C or transparent materials such as spinel.

10. References

1. Sherman, D. Impact Failure Mechanisms in Alumina Tiles on Finite Thickness Support and the Effect of Confinement. *Int. J. Impact Eng.* **2000,** *24* (3), 313–328.
2. Bourne, N.; Millett, J.; Rosenberg, Z.; Murray, N. On the Shock Induced Failure of Brittle Solids. *J. Mech. Phys. Solids* **1998**, *46* (10), 1887–1908.
3. Sherman, D.; Ben-Shushan, T. Quasi-Static Impact Damage in Confined Ceramic Tiles. *Int. J. Impact Eng.* **1998**, *21* (4), 245–265.
4. Latella, B. A.; O'Conner, B.; Padture, N. P.; Lawn, B. R. Hertzian Contact Damage in Porous Alumina Ceramics. *J. Am. Ceram. Soc.* **1997**, *80* (4), 1027–1031.
5. Anderson, C. E.; Walker, J. D.; Lankford, J. *Investigations of the Ballistic Response of Brittle Materials;* Report No. A369303; Southwest Research Institute: San Antonio, TX, 1995.
6. Singletary, J. N.; Coffelt, R. A.; Gillespie, J. W.; Gama, B. A. *Impact and High Strain Rate Response of 3-D Woven Systems;* Report No. A748883; 3Tex Fiber Products: Cary, NC, 2001.
7. Chacon-Nava, J. G.; Stott, F. H.; de la Torre, S. D.; Martinez-Villafane, A. Erosion of Alumina and Silicon Carbide at Low-Impact Velocities. *Mater. Lett.* **2002**, *55*, 269–273.
8. Bueno, S.; Micele, L.; Baudin, C.; de Portu, G. Reduced Strength Degradation of Alumina-Alumina Titanate Composite Subjected to Low-Velocity Impact Loading. *J. Eur. Ceram. Soc.* **2008**, *28*, 2923–2931.
9. Park, J. H.; Ha, S. K.; Kang, K. W.; Kim, C. W.; Kim, H. S. Impact Damage Resistance of Sandwich Structure Subjected to Low Velocity Impact. *J. Mater. Proc. Tech.* **2008**, *201*, 425–430.
10. Zhang, Z. Y.; Richardson, S. O. W. Low Velocity Impact Induced Damage Evaluation and Its Effect on the Residual Flexural Properties of Pultruded GRP Composites. *Compos. Struct.* **2007**, *81* (2), 195–201.
11. Schubel, P. M.; Luo, J.; Daniel, I. M. Low Velocity Impact Behavior of Composite Sandwich Panels. *Composites: Part A* **2005**, *36*, 1389–1396.
12. Gustin, J.; Joneson, A.; Mahinfalah, M.; Stone, J. Low Velocity Impact of Combination Kevlar/Carbon Fiber Sandwich Composites. *Compos. Struct.* **2005**, *69*, 396–406.

13. McMichael, S.; Fischer, S. Understanding Materials With Instrumented Impact. *Mech. Eng.* **1989**, 47–50.

14. Dennis, M. J. *Nondestructive Evaluation and Quality Control: Industrial Computed Tomography Metals Handbook,* 9th ed.; ASM International: Materials Park, OH, 1989; Vol. 17.

15. Stanley, J. H. *Physical and Mathematical Basis of CT Imaging,* ASTM Tutorial Section 3; ASTM CT Standardization Committee: West Conshohocken, PA, 1986.

16. Newton, T. H.; Potts, D. G. *Technical Aspects of Computed Tomography;* The C.V. Mosby Company: New York, 1981; Vol. 5.

17. Mix, P. E. *Introduction to Nondestructive Testing;* John Wiley & Sons: Portland, OR, 1987; pp 104–153.

18. Krautkramer, J.; Krautkramer, H. *Ultrasonic Testing of Materials*; Springer-Verlag: Berlin, Germany, 1990.

19. Bhardwaj, M. C. Evolution, Practical Concepts, and Examples of Ultrasonic NDC. *Ceramic Monographs – Handbook of Ceramics* **1992**, *41* (1), 188–196.

NO. OF
COPIES ORGANIZATION

1 (PDF only) DEFENSE TECHNICAL INFORMATION CTR
DTIC OCA
8725 JOHN J KINGMAN RD
STE 0944
FORT BELVOIR VA 22060-6218

1 DIRECTOR
US ARMY RESEARCH LAB
IMNE ALC HRR
2800 POWDER MILL RD
ADELPHI MD 20783-1197

1 DIRECTOR
US ARMY RESEARCH LAB
RDRL CIM L
2800 POWDER MILL RD
ADELPHI MD 20783-1197

1 DIRECTOR
US ARMY RESEARCH LAB
RDRL CIM P
2800 POWDER MILL RD
ADELPHI MD 20783-1197

ABERDEEN PROVING GROUND

1 DIR USARL
RDRL CIM G (BLDG 4600)

NO. OF COPIES	ORGANIZATION
1 (CD only)	DPTY ASST SECY FOR R&T SARD TT THE PENTAGON RM 3EA79 WASHINGTON DC 20301-7100
1	COMMANDER US ARMY TACOM AMSTA WARREN MI 48397-5000
1	PEO GCS SFAE GCS BCT M RYZYI MS 325 WARREN MI 48397-5000
2	COMMANDER US ARMY AMCOM AVN APPLIED TECH DIR J SCHUCK FT EUSTIS VA 23604-5577
1	COORS CERAMIC CO T HAEN 600 NINTH ST GOLDEN CO 80401
1	COMMANDER US ARMY TACOM AMSTA TR S L FRANKS WARREN MI 48397-5000
2	RUTGERS STATE UNIV OF NJ DEPT OF CERAMIC & MTRL ENGR R HABER A PORTUNE 607 TAYLOR RD PISCATAWAY NJ 08854

ABERDEEN PROVING GROUND

NO. OF COPIES	ORGANIZATION
30	DIR USARL RDRL SL R COATES RDRL WM S KARNA J MCCAULEY J SMITH T WRIGHT RDRL WMB J NEWILL RDRL WMM R DOWDING S MCKNIGHT RDRL WMM B K CHO RDRL WMM C R SQUILLACIOTI RDRL WMM D R BRENNAN (5 CPS) E CHIN P DEHMER G GILDE W GREEN J LASALVIA S WALSH P PATEL J SANDS RDRL WMT P BAKER C HOPPEL RDRL WMT A M BURKINS D HACKBARTH RDRL WMT B N ELDREDGE RDRL WMT C T BJERKE RDRL WMT E B RINGERS

INTENTIONALLY LEFT BLANK.